Available online at www.sciencedirect.com

ScienceDirect

Energy Procedia 114 (2017) 4872 – 4878

Energy Procedia

13th International Conference on Greenhouse Gas Control Technologies, GHGT-13, 14-18 November 2016, Lausanne, Switzerland

Pore-scale evolution of trapped CO_2 at early stages following imbibition using micro-CT imaging

Charlotte Garing[a]*, Marco Voltolini[b], Jonathan B. Ajo-Franklin[b] and Sally M. Benson[a]

[a]*Department of Energy Resources Engineering, Stanford University, 473 Via Ortega, Stanford CA 94305-2205, USA*
[b] *Lawrence Berkeley National Laboratory, Earth and Environmental Sciences, 1 Cyclotron Road, MS74R316C, Berkeley, CA 94720*

Abstract

A CO_2-brine drainage and imbibition cycle was performed in a Boise sandstone sample at reservoir conditions (1300 PSI, 44ºC) at the Advanced Light Source, LBNL. The sample was repeatedly imaged, at the pore-scale, using synchrotron-based X-ray microtomography. In particular the temporal evolution of residually trapped CO_2 was monitored for about 30 hours in order to quantify fluid stability at early stages following imbibition. The data show that fluid phase distribution distribution was not stable with time over the course of the experiment. We hypothesize that fluid displacement is caused by local capillary equilibration following the imbibition process.

Peer-review under responsibility of the organizing committee of GHGT-13.

Keywords: Carbon storage; residual trapping; micro-CT; pore-scale; high pressure experiment

1. Introduction

Despite its major influence on storage capacity, CO_2 plume migration rate, and rates of CO_2 dissolution and mineralization, there are outstanding questions regarding the mechanisms, times scales, influence of geological heterogeneity, and degree of residual trapping (Benson and Cole [1], Krevor et al., [2]). Previous studies have measured supercritical CO_2 ($scCO_2$) residual trapping at in situ conditions in order to better understand and

* Corresponding author. Tel.: +1-650-475-6051; fax: +1-650-725-2099.
E-mail address: cgaring@stanford.edu

Peer-review under responsibility of the organizing committee of GHGT-13.
doi:10.1016/j.egypro.2017.03.1628

characterize the control of the formation attributes on residual trapping and the feedbacks between residual, solubility and mineral trapping (Suekane et al. [3], Iglauer et al. [4], Krevor et al. [5], Tanino and Blunt [6], Steefel et al. [7], Andrew et al. [8]). However most experimental work have investigated residual CO_2 immediately after imbibition and also classical models of residual trapping assume that the disconnected ganglia of $scCO_2$, once pore-scale snap-off occurs, are permanently immobilized (Goodman et al. [9]). Evaluating potential phenomena that could lead to remobilization of trapped $scCO_2$, such as further dissolution in brine, wettability alteration (Kim et al. [10], Tokunaga et al. [11]) and Ostwald ripening (Schmelzer and Schweitzer [12]) is necessary to determine the permanence of residual trapping. These mechanisms could indeed alter the morphology and mobility of CO_2 droplets and consequently allow trapped ganglia to coalesce into larger ones and potentially form a continuous phase that could be mobilized by buoyancy. At shorter terms there is also a major uncertainty regarding equilibration time for the imbibition process. Previous studies pointed out non-stable fluid phase distribution after few hours suggesting that a certain time is required for equilibrium to be reached (Amstrong et al. [13]), however it has never been investigated nor quantified.

X-ray microtomography (micro-CT) is a non-destructive imaging technics that can provide high resolution images of microstructures in three dimensions (3D), allowing to visualize and better understand fluid flow in porous media at the pore scale (Wildenschild and Sheppard [14]).

The aim of the present study is to track temporal evolution of residually-trapped $scCO_2$ ganglia during the early stages following imbibition, extract critical parameters such as fluid phase connectivity and $scCO_2$ cluster size and quantify their evolution with time using synchrotron X-ray micro-CT imaging.

2. Experimental methods

2.1. Experimental set-up

The experiment was carried out in a Boise sandstone rock core with a 9 mm diameter and a length of 25 mm. The porosity measured in laboratory using a helium pycnometer on other Boise rock samples is estimated around 0.27, and mercury injection capillary pressure analysis indicate a mean pore-throat diameter of 30 µm and an entry pressure of approximately 3000 Pa for water/$scCO_2$ at 1300 PSI and 50ºC. The dry sample was placed in a tri-axial high-pressure and controlled temperature flow cell after being wrapped in a series of PTFE, aluminium and PVDF layers, in that order. The cell was then mounted vertically on the rotational stage of the microtomography beamline 8.3.2 of the Advanced Light Source (Lawrence Berkeley National Laboratory) and connected to the rest of the circuit by stainless steel tubing that could be disconnected from the cell at the inlet and outlet valves when tomography scans were acquired (Fig. 1). Pressure in the set-up was monitored using the Teledyne Isco syringe pumps transducers and temperature, for the flow cell, was controlled using a water-bath circulator. A confining pressure higher than the pore pressure was set over the course of the experiment to ensure a strong fit of the wrapping layers to the sample forcing fluid flow through the rock core. The experiment was performed using supercritical CO_2 ($scCO_2$) provided by connecting a gas cylinder to the injecting pump, and a solution of potassium iodide (KI) with a salinity of 0.75 $mol.kg^{-1}$ referred to as brine. To avoid any CO_2 dissolution in brine and ensure complete multiphase flow from the very beginning of drainage, and then imbibition, the brine was pre-equilibrated with CO_2 at the same pressure and temperature conditions of the experiment by mixing both fluids together in a Parr stirred heated reactor connected to both the gas cylinder and the injecting pump. The different fluids were injected from the bottom to the top of the flow cell to a back pressure pump set at the pressure of the experiment.

2.2. Drainage and imbibition

Once the flow cell was mounted in place, the confining pressure was increased to 300 PSI and a first scan of the dry sample at room pressure and temperature was taken for detailed pore structure analysis purpose. The sample was then first saturated with water by first injecting more than 10 pore volumes of CO_2 at 5 $mL.min^{-1}$ to replace the air with CO_2 and then injecting deionized water at 2 $mL.min^{-1}$ for 40 minutes to dissolve the CO_2 and saturate the pore

space. The water was then replaced by the CO_2-saturated brine, which was prepared by mixing the brine and $scCO_2$ in the reactor at 1300 PSI and 50ºC during 8 hours. A volume of 50mL was injected at 2 mL.min^{-1} after pressurizing the cell to 1300 PSI with a confining pressure of 1500 PSI and setting the temperature to 50ºC. The brine-saturated sample was scanned prior to drainage (Fig. 2.a)).

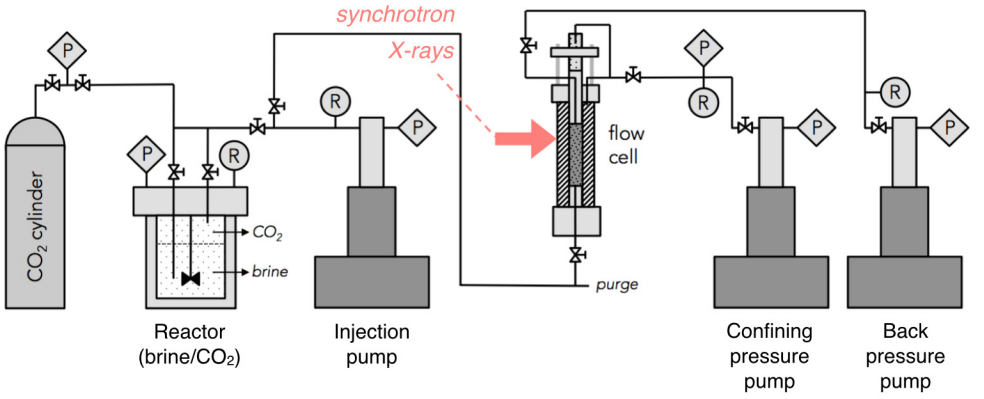

Fig. 1. Experimental set-up to perform high pressure CO_2-brine core flooding at the X-ray microtomography beamline of the Advanced Light Source (ALS – Beamline 8.3.1) at Lawrence Berkeley National Laboratory

The injection pump was then emptied and filled with CO_2 at 1300 PSI and 80 mL was injected at a flow rate of 2 mL.min^{-1}. The sample was scanned after drainage prior to imbibition (Fig. 2.b)). The injecting pump was filled again with CO_2-saturated brine from the mixing reactor and 80 mL was injected at 2 mL.min^{-1}, as previously. The sample cell was then isolated and the sample was scanned multiple times after stopping the brine injection: after 3 hours (Fig. 2.c.)), 8 hours, 16 hours and 31 hours (Fig. 2.d)).

For the experimental conditions listed above, the flow is laminar ($N_{Re} \sim 1$) and capillary forces should dominate over viscous or buoyancy forces ($N_C \sim 10^{-7}$, $N_B \sim 10^{-3}$), with N_{Re}, N_C and N_B being the packed beds Reynolds number, Capillary number and Bond number, respectively, defined as follow:

$$N_{Re} = d_g Q\rho / A\mu(1-\phi),\ N_C = Q\mu/A\gamma \text{ and } N_B = \Delta\rho g {d_p}^2/\gamma,$$

with Q the flow rate, ρ the density, μ the viscosity, γ the interfacial tension, A the cross section, ϕ the porosity, and d_g and d_p the grain and pore diameter (Table 1).

Table 1. Properties of the rock sample and fluids at the experimental conditions of 1300 PSI and 44ºC ([a]NIST chemistry web book, [b]From Krevor et al. [15] for scCO2/water at 1300 PSI-50ºC, [c]From Pini and Benson [16] for scCO2/brine (2.5 mol.kg^{-1}) at 1300 PSI-50ºC)

A (m^2)	6.36E^{-5}
ϕ (–)	0.27
d_g - d_p (µm)	150 – 50
ρ_{nw} (kg.m^{-3})	349 [a]
ρ_w (kg.m^{-3})	995 [a]
μ_{nw} (10^{-5} Pa.s)	2.6 [a]
μ_w (10^{-5} Pa.s)	61
γ (mN.m^{-1})	37[b] – 41[c]

2.3. Image acquisition and analysis

For each step (dry, brine, drainage, 4 imbibition times) the core was imaged by performing two scans, one of the top and the other of bottom of the sample, that overlap over 200 pixels in the middle of the sample. The data acquisition was carried out using filter-hardened polychromatic X-rays from the source (superbend magnet), and a detector system comprising a 50 µm LuAG scintillator, a 2x microscope objective optics system, and a PCO Edge CCD camera. For each scan, a set of 2049 projections over a 180º rotation were collected, with an exposure time of 225 ms. The tomographic reconstruction was carried out using a conventional filtered back-projection algorithm (Dierick et al. [17]) yelding 2500*2500*1200 voxels^3 volumes, with a (isotropic) voxel size of 3.24 µm.

The two overlapping volumes imaging the core at one specific time were binned x2 and merged, resulting in volumes of 1300*1300*1110 voxels^3 with a voxel size of 6.48 µm. A full porosity analysis (porosity quantification, connectivity and pore equivalent diameter) was performed using the dry scan. The same analysis was also conducted on a sub-volume of 800^3 voxels^3 extracted from the original image (3.24 µm voxel size) and from the binned one (6.48 µm voxels size) in order to investigate the effect of binning. All results were very similar yielding a total porosity of 0.23 connected at 99.5%, with a mean pore diameter around 45 µm.

Each merged volumes were registered to the first imbibition scan, taken as reference, using a normalized mutual information metric and then resampled on a same grid using a Lanczos filter for interpolation. The volumes can then be compared by analyzing the difference images in between two volumes (subtraction of one image from an other image) leading to accurate quantification of fluid phase (CO_2 and brine) changes in between the two images (Fig. 2.e)). Each volume can also be analyzed separately. The CO_2 phase was identified using a seeded watershed segmentation algorithm (Fig. 2.f)) and the separated CO_2 ganglia were then labeled (Fig. 2.g) and h)) and analyzed.

All image analysis was done using imageJ and PerGeos (FEI) programs.

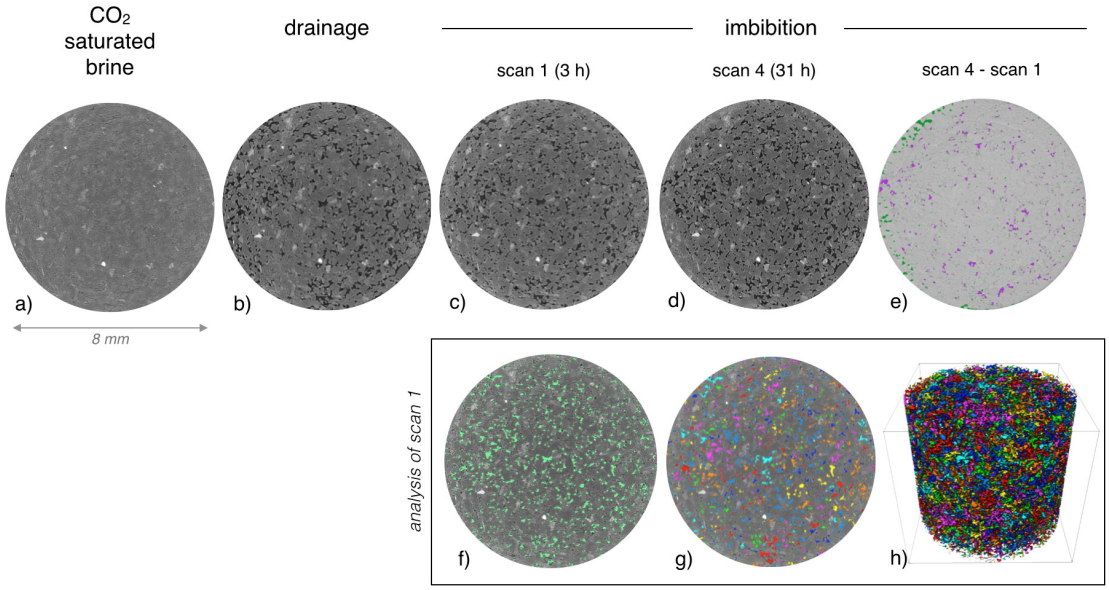

Fig. 2. Cross section through the 3D reconstructed volumes of the sample imaged a) after saturation with CO_2-saturated brine, b) after drainage, c) 3 hours after imbibition and d) 31 hours after imbibition; c) 2D overlay of segmented lost CO_2 (green) and gained CO_2 (purple) in between 3 and 31 hours on the difference image; 2D overlay of f) segmented CO_2 and g) labeled CO_2 ganglia of the first imbibition scan (after 3 hours) and h) 3D visualization of the labeled ganglia.

3. Results and discussion

The analysis of the scan acquired after drainage shows that $scCO_2$ forms a highly connected phase, with one large cluster representing 97% of the entire phase (Fig. 3.a)) and saturating 45% of the pore space (Fig. 4.a)). The first scan taken 3 hours after imbibition shows that residual CO_2 saturates the pore structure more homogeneously (Fig. 3.b), with a lower value of approximately 0.41 (Fig. 4.a)). The results also show that the CO_2 phase consists in a higher number of separated ganglia of smaller size (Fig. 4.b)). This is in good agreement with previous studies about residual trapping in reservoir rocks confirming that the imbibition process significantly disconnects the non wetting phase leading to CO_2 ganglia of various size with most ganglia localized in few pores (Iglauer et al. [3], Andrew et al. [7]). The analysis of residual $scCO_2$ at longer times after imbibition shows that although the overall saturation stay stable around 0.40 (Fig. 4.a)), there is noticeable changes in the phase distribution. There are less $scCO_2$ ganglia with time and the mean ganglia size increases (Fig. 3.a to e)), Fig. 4.b)).

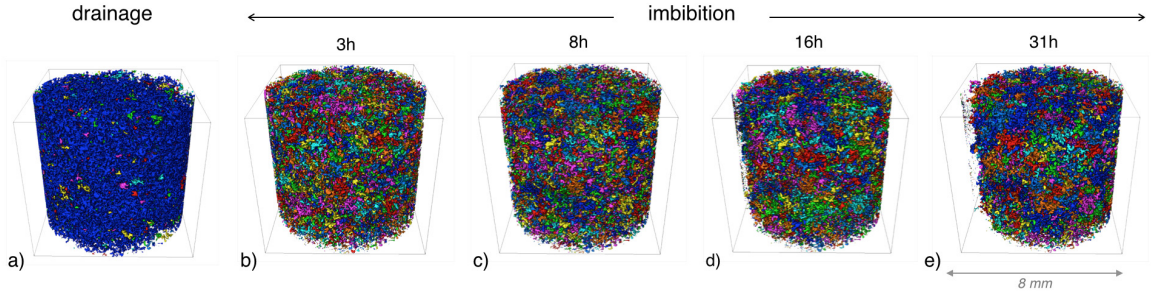

Fig. 3. 3D visualization of CO_2 ganglia a) after drainage and at b) 3 hours, c) 8 hours, d) 16 hours and e) 31 hours after imbibition. Separated ganglia are represented with different colors.

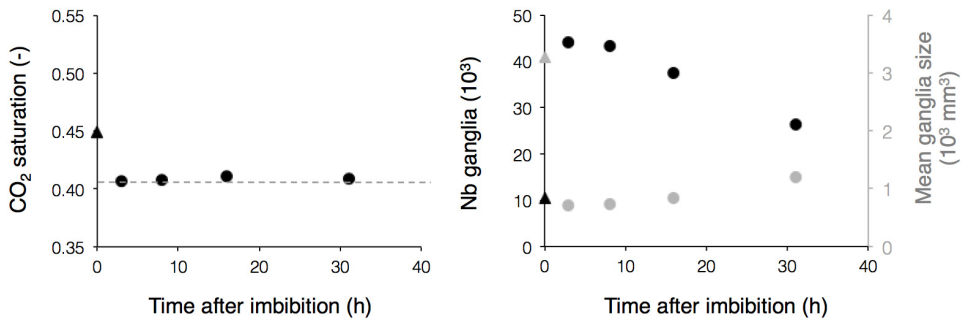

Fig. 4. Temporal evolution of a) CO2 saturation and b) the number of ganglia (black symbols) and mean ganglia size (grey symbols) after imbibition. The triangle symbols at 0h represent the drainage data and the circles symbols represent the data for different times after imbibition.

Residual CO_2 displacement over time was investigated by comparing the images acquired during the day following imbibition to the first one acquired 3 hours after imbibition. The results are displayed in Fig. 5. They

suggest a lateral movement of CO_2 rather than a vertical one which could be driven by buoyancy forces. The data shown in the previous paragraph suggest indeed the formation of larger size ganglia over time that could be more easily remobilized upward. However this is not seen in the dataset. The results more likely suggest that capillary re-equilibrium due to small scale heterogeneity is occurring once imbibition stops. While the experiment is conducted at capillary numbers such that capillary forces dominate over viscous forces, we hypothesize the ratio of capillary to viscous forces is not be sufficient to achieve capillary equilibrium throughout the heterogeneous core plug while imbibition is occurring. Further work is ongoing to test this hypothesis.

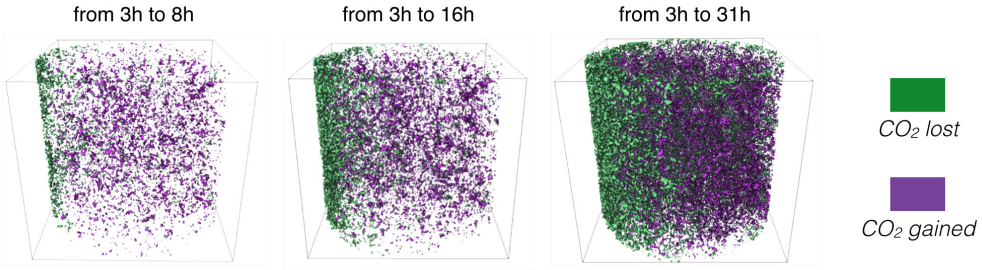

Fig. 5. Visualization of CO_2 displacement between the different scans acquired after imbibition and the first scan taken 3 hours after imbibition. The lost CO_2 (CO_2 replaced by brine) is displayed in green and the gained CO_2 (brine replaced by CO_2) is displayed in purple.

5. Conclusion

We performed one cycle of $scCO_2$-brine drainage and imbibition core floods on a Boise sandstone rock sample at a synchrotron beamline allowing to image fluid phase distribution over the course of the experiment. A particular attention was drawn to the temporal evolution of residual $scCO_2$ during the day following imbibition. This unique experiment highlights noticeable fluid displacement after imbibition and show that fluid phase distribution is still not stable 30 hours after brine injection stops. In particular the results show that the isolated ganglia formed by the imbibition process tend to get reconnected over time, progressively forming larger size ganglia. No buoyancy effects were seen in that experiment. We hypothesize that residual $scCO_2$ is getting redistributed to reach capillary equilibrium consistent with local variations in the morphology of the pore space after imbibition stops.

Acknowledgements

This research was supported by the Center for Nanoscale Control of Geologic CO_2, an Energy Frontier Research Center funded by the U.S. Department of Energy, under contract number DE-AC02-05CH11231. C. Garing and S.M. Benson also acknowledge support from The Global Climate and Energy Project (GCEP) at Stanford. Micro-tomographic imaging was performed with the assistance of Alastair MacDowell and Dula Parkinson at the Advanced Light Source, Beamline 8.3.2, supported by the U.S. DOE Office of Science, Office of Basic Energy Sciences (DE-AC02-05CH11231).

References

[1] Benson SM and Cole DR. CO_2 sequestration in deep sedimentary formations. Elements; 2008; 4(5):325–331.
[2] Krevor S, Blunt MJ, Benson SM, Pentland CH, Reynolds C, Al-Menhali A, and Niu B. Capillary trapping for geologic carbon dioxide storage–From pore scale physics to field scale implications. International Journal of Greenhouse Gas Control; 2015; 40:221-237.
[3] Suekane T, Nobuso T, Hirai S, and Kiyota M. Geological storage of carbon dioxide by residual gas and solubility trapping. International Journal of Greenhouse Gas Control; 2008; 2:58-64.
[4] Iglauer S, Paluszny A, Pentland CH, and Blunt MJ. Residual CO_2 imaged with X-ray micro-tomography. Geophysical Research Letters 2011; 38(21).

[5] Krevor SCM, Pini R, Li B, and Benson SM. Capillary heterogeneity trapping of CO_2 in a sandstone rock at reservoir conditions. Geophysical Research Letters; 2011; 38:L15401, doi:10.1029/2011GL048239,2011.
[6] Tanino Y and Blunt MJ. Capillary trapping in sandstones and carbonates: Dependence on pore structure. Water Resources Research 2012; 48(8):1–13.
[7] Steefel CI, Molins S, and Trebotich D. Pore scale processes associated with subsurface CO2 injection and sequestration. Reviews in Mineralogy and Geochemistry; 2013; 77:259-303.
[8] Andrew M, Bijeljic B, and Blunt MJ. Pore-scale imaging of trapped supercritical carbon dioxide in sandstones and carbonates. International Journal of Greenhouse Gas Control; 2014; 22:1-14.
[9] Goodman A, Hakala A, Bromhal G, Deel D, Rodosta T, Frailey S, Small M, Allen D, Romanov V, Fazio J, Huerta N, McIntyre D, Kutchko B, and Guthrie G. US DOE methodology for the development of geologic storage potential for carbon dioxide at the national and regional scale. International Journal of Greenhouse Gas Control; 2011; 5:952-965.
10] Kim Y, Wan J, Kneafsey TJ, and Tokunaga TK. Dewetting of silica surfaces upon reactions with supercritical CO_2 and brine: Porescale studies in micromodels. Environ. Sci. Technol.; 2012; 46:4228-4235.
[11] Tokunaga T, Wan J, Jung JW, Kim TW, Kim Y and Dong W. Capillary pressure and saturation relations for supercritical CO_2 and brine in sand: High-pressure *Pc(Sw)* controller/meter measurements and capillary scaling predictions. Water Resources Research; 2013; 49:4566-4579.
[12] Schmelzer J, and Schweitzer F.1987. Ostwald Ripening of Bubbles in Liquid-Gas Solutions. J. Non-Equilibrium Thermodyn; 1987; 12(3):255-270.
[13] Armstrong RT, Porter ML, and Wildenschild D. Linking pore-scale interfacial curvature to column-scale capillary pressure. Advances in Water Resources; 2012; 46:55-62.
[14] Wildenschild D, and Sheppard A P. X-ray imaging and analysis techniques for quantifying pore-scale structure and processes in subsurface porous medium systems. Advances in Water resources; 2013; 51:217-246.
[15] Krevor S, Pini R, Zuo L, and Benson SM. Relative permeability and trapping of CO_2 and water in sandstone rocks at reservoir conditions. Water Resources Research; 2012; 48:W02532.
[16] Pini R, and Benson SM. Simultaneous determination of capillary pressure and relative permeability curves from core-flooding experiments with various fluid pairs. Water Resources Research; 2013; 49:3516-3530.
[17] Dierick M, Masschaele B, and Van Hoorebecke L. Octopus, a fast and user-friendly tomographic reconstruction package developed in LabView®. Measurement Science and Technology; 2004;15:1366-1370.